CAMBRIDGE
UNIVERSITY PRESS

Article

Structural factors affecting the crystal-chemical variability in Al-rich K-dioctahedral $2M_1$ micas

Bella B. Zviagina* and Victor A. Drits

Geological Institute of the Russian Academy of Sciences, 7 Pyzhevsky per., 119017 Moscow, Russia

Abstract

To reveal the factors that determine the different ranges of compositional variations in high- and low-temperature Al-rich K-dioctahedral micas, relationships between structural parameters and cation composition were analysed for: (1) a series of synthetic $2M_1$ muscovite–phengite–aluminoceladonite samples; and (2) Al-rich, K-dioctahedral $2M_1$ micas with previously published refined structural data. The dependences of the unit-cell parameters on cation composition and the variations in tetrahedral and octahedral lateral dimensions and sheet thicknesses, interlayer distances and tetrahedral rotation angles were analysed and compared with those found previously for the series $1M$ *trans*-vacant (*tv*) illite–$1M$ aluminoceladonite. The similarities in the variations of unit-cell parameters with cation composition observed in $2M_1$ and $1M$ natural and synthetic K-dioctahedral micas imply that these variations are controlled by similar – albeit not identical – structural factors. A major structural factor is the readjustment of the differently sized tetrahedral and octahedral sheets, which is realized in a different manner in micas formed under different pressure and temperature conditions.

The solid solution from muscovite, $KAl_2(Si_3Al)O_{10}(OH)_2$, to aluminoceladonite, $KAl(Mg,Fe)Si_4O_{10}(OH)_2$, is one of the basic composition series conventionally distinguished in K-dioctahedral micas (Rieder *et al.*, 1998). Natural high- and low-temperature Al-rich K-dioctahedral micas, however, differ in the ranges of compositional variations. High-temperature K-dioctahedral $2M_1$ and $3T$ micas only form a series between muscovite and the intermediate member phengite, $KAl_{1.5}Mg_{0.5}(Si_{3.5}Al_{0.5})O_{10}(OH)_2$ (Bailey, 1984; Brigatti & Guggenheim, 2002; Ferraris & Ivaldi, 2002). Micas of muscovite-like compositions with 3.0–3.3 Si cations per half formula unit (phfu) occur in granitoides and in greenschists or low to intermediate amphibolite facies (low-pressure Barrow-type metamorphism). Phengites having Si contents of 3.3–3.6 cations phfu are formed during high-pressure metamorphism, such as blueschist or eclogite facies (Schmidt *et al.*, 2001). Neither $2M_1$ nor $3T$ aluminoceladonites have been found in nature; dioctahedral Al,Mg-bearing mica samples consisting of $2M_1$ and/or $3T$ polytypes with >3.8 Si cations phfu were only synthesized at extremely high temperatures and pressures (at ~700–900°C and 10–11 GPa; Domanik & Holloway, 1996; Smyth *et al.*, 2000; Schmidt *et al.*, 2001). In a few instances, samples with a phengite-like composition were called aluminoceladonites (*e.g.* Pe-Piper, 1985; Ripp *et al.*, 2009; Beyer *et al.*, 2010), probably because of a certain ambiguity and controversy in the existing nomenclature of micas.

In contrast, low-temperature Al-rich K-dioctahedral micas, which normally occur as finely dispersed, mostly interlayer-deficient $1M$ and $1M_d$ varieties, form a continuous series from illite to aluminoceladonite (Środoń & Eberl, 1984; Drits & Kossovskaya, 1991; Brigatti & Guggenheim, 2002; Drits *et al.*, 2006, 2010; Wilson, 2013; Zviagina *et al.*, 2015). All natural aluminoceladonite samples known to date are $1M$ polytypes that formed at relatively low temperatures (up to 200°C) and pressures, mostly under the action of highly mineralized solutions in evaporite basins (Seifert, 1968; Sokolova *et al.*, 1976; Rasskazov, 1984; Drits & Kossovskaya, 1991; Petrova & Amarjargal, 1996; Murao *et al.*, 2009; Drits *et al.*, 2010; Środoń *et al.*, 2013). Drits *et al.* (2006) analysed the structural and crystal-chemical factors that control the occurrence and relative stability, under the given physicochemical conditions, of *cis*-vacant (*cv*) and *trans*-vacant (*tv*) layers in dioctahedral 2:1 phyllosilicates. In particular, they showed that the interlayer arrangement in *tv* $1M$ micas, where the grooves formed by the rows of the depressed oxygen anions in the basal tetrahedral surfaces across the interlayer have the same orientation, should be less favourable than that in *cv* $1M$ micas, where the tetrahedral sheets across the interlayer are rotated by 120° with respect to each other. The latter arrangement, which is similar to that in *tv* $2M_1$ micas, ensures reduced differences between individual K–O bond lengths and minimization of repulsion of the basal oxygen anions across the interlayer. On the other hand, the symmetrical arrangement of the octahedral sheet should stabilize the *tv* structure as compared to the *cv* structure. Decreasing contents of tetrahedral and octahedral Al and increasing contents of larger octahedral Mg and Fe cations lead to a decrease in the tetrahedral rotation and corrugation, as well as a decrease in the size difference between the occupied

*E-mail: zbella2001@yahoo.com

and vacant octahedra. As a result, the role of the symmetry of the octahedral sheet begins to prevail over that of the interlayer structure. Therefore, Fe-rich and Mg-rich dioctahedral micas (Mg-rich illites, aluminoceladonites, Fe-illites, Al-glauconites, glauconites and celadonites) always occur as *tv* varieties, whereas (Mg, Fe)-poor illites can have either *tv* or *cv* structures (Drits *et al.*, 2006; Zviagina *et al.*, 2015, 2017).

Factors controlling the occurrence of the various polytypes of high-pressure K-dioctahedral micas have been analysed by several authors. Velde (1965) suggested that $2M_1$ is the most stable phengite polytype and that an important role in polytype stability is played by kinetics. Stöckert (1985) suggested that the $3T$ polytype is more common in Mg-rich phengites, which contain at least a minor amount of Fe and/or Na, whereas the $2M_1$ polytype may be more typical for Mg-poor compositions. Sassi *et al.* (1994) and Curetti *et al.* (2008) suggested that high-pressure conditions may favour the $3T$ over the $2M_1$ polytype, and Sassi *et al.* (2010) concluded that the growth of the $3T$ polytype was not a function of mica composition. The synthetic micas in the muscovite–phengite–aluminoceladonite series (Schmidt *et al.*, 2001) contain 60–100% of the $2M_1$ polytype, 3–40% of the $1M$ polytype and 5–26% of the $3T$ polytype. The $3T$ polytype was only present in three samples synthesized at ≥800°C and ≥8 GPa. There was no clear dependence of the presence or abundance of any polytype on the Si and Mg contents; the three $3T$-bearing samples, however, had ≥3.8 Si and ≥0.85 Mg cations phfu. Unlike Massonne & Schreyer (1986), who observed decreases in the $2M_1$ and increases in the $1M$ polytype contents with decreasing pressure, temperature, and Mg contents in the 'white mica' samples synthesized at ~400–800°C and ~0.3–3.0 GPa, Schmidt *et al.* (2001) observed no correlation between the estimated abundance of the $1M$ polytype and any of the controlled experimental variables in the muscovite–phengite–aluminoceladonite samples synthesized at ~700–1000°C and 2–10 GPa. This discrepancy may be associated with the differences in the experimental conditions (particularly the much higher pressures used by Schmidt *et al.*, 2001). Schmidt *et al.* (2001) concluded that kinetics and/or other uncontrolled experimental variables may play a major role in polytype stabilization.

To date, no explanation has been found for the different composition variation ranges in high-temperature Al-rich K-dioctahedral $2M_1$ and $3T$ micas and low-temperature $1M$ varieties. The objective of the present study was to reveal the structural and compositional factors that prevent the formation of high-temperature $2M_1$ aluminoceladonite and favour the formation of relatively low-temperature $1M$ aluminoceladonite. For this purpose, the relationships between structural parameters and cation composition were analysed for two groups of samples: (1) a series of synthetic $2M_1$ muscovite–phengite–aluminoceladonite samples of Schmidt *et al.* (2001) (Tables 1, 2); and (2) Al-rich, K-dioctahedral $2M_1$ micas with previously published refined structural data (Tables 3, 4). $3T$ muscovite–phengite micas were not considered because of the scarcity of experimental data, and also because they would have overcomplicated the analysis. For the same reason, mixtures of $1M$ and $2M_1$ polytypes, which occur, for example, in fine-grained aggregates of mica-like phases previously called 'sericites', were not considered either. For both sets of samples, dependences of the unit-cell parameters on cation composition were analysed and compared with those found for the series of $1M$ *tv* illite–aluminoceladonite by Zviagina *et al.* (2015). In addition, the variations in tetrahedral and octahedral lateral dimensions and sheet thicknesses, interlayer distances and tetrahedral

Table 1. Cation compositions of synthetic $2M_1$ micas in the series muscovite–phengite–aluminoceladonite (per $O_{10}(OH)_2$) (Schmidt *et al.*, 2001).

Sample	Si	^{IV}Al	^{VI}Al	Mg	Σ_{oct}	K
P13-1	3.987	0.013	1.021	0.974	1.995	1.000
P17	3.947	0.053	1.053	0.957	2.010	0.978
P11-2	3.823	0.177	1.135	0.838	1.973	0.973
P18-2	3.817	0.183	1.187	0.809	1.996	1.000
P12-1	3.662	0.338	1.341	0.662	2.003	0.994
P15	3.642	0.358	1.352	0.654	2.006	0.995
P28	3.478	0.522	1.574	0.416	1.990	0.968
P25	3.401	0.599	1.578	0.442	2.020	0.981
P33	3.288	0.712	1.708	0.308	2.016	0.971
P30	3.219	0.781	1.770	0.249	2.019	0.973
P26	3.176	0.824	1.773	0.292	2.065	0.923
P31	3.124	0.876	1.918	0.108	2.026	0.907
P29	3.113	0.887	1.908	0.097	2.005	0.968

Σ_{oct} = sum of octahedral cations.

Table 2. Unit-cell parameters of synthetic $2M_1$ micas in the series muscovite–phengite–aluminoceladonite (Schmidt *et al.*, 2001).

Sample	a (Å)	b (Å)	c (Å)	β (°)	$c\sin\beta$ (Å)	$c\cos\beta/a$	% $2M_1$
P13-1	5.207(7)	9.016(2)	19.852(3)	95.54(2)	19.759	−0.368	88.2
P17	5.206(2)	9.019(3)	19.871(2)	95.42(2)	19.782	−0.360	100
P11-2	5.213(2)	9.021(4)	19.877(2)	95.60(2)	19.782	−0.372	87.2
P18-2	5.210(4)	9.028(6)	19.888(3)	95.59(3)	19.793	−0.372	83.7
P12-1	5.211(1)	9.032(1)	19.916(1)	95.62(1)	19.820	−0.374	79.3
P15	5.213(2)	9.031(4)	19.914(6)	95.64(2)	19.818	−0.375	100
P28	5.2039(6)	9.024(1)	19.978(1)	95.75(1)	19.878	−0.385	94.8
P25	5.209(2)	9.026(3)	19.998(2)	95.80(2)	19.896	−0.388	100
P33	5.2025(4)	9.022(7)	20.031(1)	95.76(1)	19.930	−0.386	97.2
P30	5.1988(8)	9.015(1)	20.074(2)	95.75(1)	19.973	−0.387	86.1
P26	5.2037(5)	9.0250(9)	20.069(1)	95.75(2)	19.968	−0.386	94.5
P31	5.1876(6)	8.998(1)	20.091(1)	95.77(2)	19.989	−0.389	100
P29	5.1886(8)	8.997(1)	20.108(2)	95.79(2)	20.005	−0.391	100

rotation angles were considered for the refined structures (group 1) and for structure models of synthetic samples (group 2) obtained using the structure modelling algorithm of Zviagina & Drits (2012).

Initial data and methods

Two sets of data were analysed for relationships between structural characteristics and cation composition. The series of micas in the muscovite–aluminoceladonite join synthesized by Domanik & Holloway (1996) and analysed for polytype contents and unit-cell parameters by Schmidt *et al.* (2001) (group 1, Tables 1, 2) are ideal for such analysis, as the composition variation in the series is solely determined by the coupled heterovalent Tschermak substitution $^{VI}Al^{IV}Al \leftrightarrow {}^{VI}Mg^{IV}Si$. Moreover, the K content is close to 1 cation phfu in all the samples, which minimizes the potential influence of the interlayer cation composition. The 13 samples selected for the analysis were those with the greatest contents of the $2M_1$ polytype (79.3–100%; Table 2) and the sum of octahedral cations, Σ_{oct}, closest to 2 cations phfu (1.97–2.06; Table 1). The Si and Mg contents in the group 1 samples range from 3.11 to 3.99 cations phfu and from 0.10 to 0.97 cations phfu, respectively, so that five samples have muscovite and near-muscovite compositions, four samples have phengite-like compositions and four samples have aluminoceladonite and aluminoceladonite-like compositions (Table 1).

Group 2 comprises refined structural data of 18 natural micas (muscovites, phengitic muscovites and phengites) and one aluminoceladonite synthesized by Domanik & Holloway (1996) and refined by Smyth *et al.* (2000) (see Table 3 for cation compositions and

Table 3. Cation compositions (atoms phfu) of $2M_1$ micas with refined structures (natural muscovites and phengites and synthetic aluminoceladonite).

#	Sample	Si	^{IV}Al	^{VI}Al	Fe^{3+}	Fe^{2+}	Mg	Ti	Mn^{3+}	Mn^{2+}	Cr	K	Na	Ca	Ba	Σ_{oct}	Reference
1	Muscovite – $2M_1$	3.12	0.88	1.88	–	0.14	0.01	–	–	–	–	0.85	0.09	–	–	2.03	Rothbauer (1971)
2	Muscovite – $2M_1$	3.06	0.94	1.72	0.15	–	0.10	0.02	0.02	–	–	0.93	0.05	–	–	2.01	Knurr & Bailey (1986)
3	Muscovite – $2M_1$	3.16	0.84	1.84	0.06	0.01	0.10	–	–	–	–	0.79	0.04	0.03	–	2.01	Tsipursky & Drits (1977)
4	Muscovite – $2M_1$	3.02	0.98	1.90	0.02	0.05	0.06	0.01	–	–	–	0.86	0.10	–	–	2.04	Güven (1971)
5	Muscovite – $2M_1$ (Keystone)	3.10	0.90	1.83	–	0.16	0.01	–	–	–	–	0.93	0.06	0.01	–	2.00	Guggenheim *et al.* (1987)
6	Muscovite – $2M_1$ (Westland)	3.11	0.89	1.86	–	0.04	0.08	–	–	–	0.06	0.86	0.01	–	0.04	2.04	Brigatti *et al.* (2001)
7	Muscovite – $2M_1$ (B1b)	3.09	0.91	1.83	–	0.07	0.07	0.06	–	–	–	0.94	0.06	–	–	2.03	Brigatti *et al.* (1998)
8	Muscovite – $2M_1$ (C3-29b)	3.07	0.93	1.88	–	0.07	0.06	0.03	–	–	–	0.88	0.06	0.06	–	2.04	Brigatti *et al.* (1998)
9	Muscovite – $2M_1$ (GFS-15)	3.03	0.97	1.86	0.01	0.06	0.07	0.02	–	–	–	0.92	0.08	–	–	2.02	Brigatti *et al.* (1998)
10	Muscovite – $2M_1$ (H87b)	3.09	0.91	1.71	0.16	0.13	–	–	–	0.01	–	0.96	0.04	–	–	2.01	Brigatti *et al.* (1998)
11	Muscovite – $2M_1$ (A4b)	2.92	1.08	1.88	0.09	–	0.05	0.02	–	–	–	0.92	0.08	–	–	2.04	Brigatti *et al.* (1998)
12	Muscovite – $2M_1$ (C3-31b)	3.18	0.82	1.64	0.08	0.08	0.16	0.02	–	–	–	0.93	0.05	0.01	–	1.98	Brigatti *et al.* (1998)
13	Muscovite – $2M_1$ (RA1)	3.18	0.82	1.78	–	0.12	0.06	0.04	–	–	–	0.92	0.08	–	–	2.00	Brigatti *et al.* (1998)
14	Fe-rich muscovite – $2M_1$ (GA1)	3.30	0.70	1.65	–	0.29	–	0.01	–	0.07	–	0.99	0.01	–	0.01	2.02	Brigatti *et al.* (1998)
15	Fe-rich muscovite – $2M_1$	3.26	0.74	1.67	–	0.34	0.04	–	–	–	–	0.94	0.03	–	–	2.05	Pavese *et al.* (1999)
16	Mg-rich muscovite – $2M_1$	3.25	0.75	1.51	–	0.15	0.27	0.01	–	–	0.09	0.95	0.05	–	–	2.03	Rule & Bailey (1985)
17	Phengite – $2M_1$ (2M1Y)	3.38	0.62	1.55	–	0.21	0.24	0.02	–	–	–	0.98	0.02	–	–	2.02	Ivaldi *et al.* (2001)
18	Phengite – $2M_1$ (2M1G)	3.45	0.55	1.42	–	0.24	0.33	0.04	–	–	–	0.98	0.02	–	–	2.03	Ivaldi *et al.* (2001)
19	Aluminoceladonite – $2M_1$	3.81	0.19	1.21	–	0.04	0.75	–	–	–	–	1.00	–	–	–	2.00	Smyth *et al.* (2000)

Σ_{oct} = sum of octahedral cations.

Table 4. Unit-cell parameters of refined $2M_1$ mica structures[a] (natural muscovites and phengites and synthetic aluminoceladonite).

#	a (Å)	b (Å)	c (Å)	β (°)	$c\sin\beta$ (Å)	$c\cos\beta/a$
1	5.1918(2)	9.0155(3)	20.0457(5)	95.735(2)	19.945	−0.386
2	5.2044(8)	9.018(2)	20.073(5)	95.82(2)	19.970	−0.391
3	5.190(2)	9.000(2)	20.048(3)	95.73(3)	19.948	−0.386
4	5.1906(2)	9.0080(3)	20.0470(6)	95.757(2)	19.946	−0.387
5	5.200(4)	9.021(7)	20.07(2)	95.71(7)	19.970	−0.384
6	5.192(1)	9.011(1)	20.028(2)	95.74(1)	19.928	−0.386
7	5.187(2)	9.004(2)	20.036(2)	95.73(2)	19.936	−0.386
8	5.188(1)	8.996(3)	20.082(2)	95.78(1)	19.980	−0.390
9	5.192(2)	9.013(5)	20.056(7)	95.83(3)	19.952	−0.392
10	5.209(3)	9.035(6)	20.066(9)	95.68(3)	19.967	−0.381
11	5.186(1)	8.991(3)	20.029(7)	95.77(3)	19.928	−0.388
12	5.197(1)	9.022(3)	20.076(4)	95.79(2)	19.974	−0.390
13	5.182(3)	8.982(5)	20.002(5)	95.72(2)	19.902	−0.385
14	5.226(1)	9.074(2)	20.039(2)	95.74(1)	19.939	−0.383
15	5.21397(6)	9.0521(1)	19.9968(2)	95.736(1)	19.897	−0.383
16	5.2153(5)	9.043(2)	19.974(9)	95.789(9)	19.872	−0.386
17	5.2132(8)	9.051(2)	19.937(5)	95.76(2)	19.836	−0.384
18	5.225(1)	9.057(2)	19.956(6)	95.73(2)	19.856	−0.381
19	5.2046(8)	9.0368(16)	19.886(4)	95.615(14)	19.791	−0.374

[a] Sample numbers as in Table 3.

references to structural data, and see Table 4 for unit-cell parameters). The data were selected according to the same criteria as in Zviagina & Drits (2012): high precision in the published structural data ($R < 10\%$); Σ_{oct} from 1.9 to 2.1 cations phfu; overall cation charge phfu from 21.85 to 22.15; Li and/or F < 0.25 atoms phfu. The synthetic sample of Smyth *et al.* (2000) was included in group 2 as it is the only refined $2M_1$ aluminoceladonite structure reported to date.

The results obtained for the $2M_1$ mica structures were compared with those for $1M$ micas in the illite–aluminoceladnite series studied by Drits *et al.* (2010) and Zviagina *et al.* (2015).

Regression analysis

Regression equations relating unit-cell parameters with cation composition were obtained using the standard procedures in MS Excel. The quality of the regressions was evaluated based on the coefficient of determination, R^2, estimated standard deviation values, *esd*, and ANOVA quality-of-fit *p*-values. Conventionally, the acceptable level of significance of a regression corresponds to $R^2 \geq 0.8$ and $p \leq 0.05$. The acceptable *esd* values should be comparable with the precision in the experimental structure determinations (*i.e.* ≤0.01 Å for distance parameters).

Structure modelling

As Schmidt *et al.* (2001) did not refine the structures of synthetic micas (group 1), the algorithm of Zviagina & Drits (2012) was used to calculate the unit-cell atomic coordinates from the data on unit-cell parameters and cation composition (Supplementary Table S1). The *esd* values for the modelled *x*, *y* and *z* coordinates vary for different atomic positions and range from 0.0001 to 0.003 (fractional units). The *esd* values for the structure details obtained from the calculated atomic coordinates are 0.002–0.007 Å for mean and individual tetrahedral bond and edge lengths, 0.004–0.013 Å for mean and individual octahedral bond and edge lengths, 0.013–0.015 Å for K–O distances and 0.5° for the tetrahedral ditrigonal rotation angle, α_{tet}. The structure parameters for the $1M$ micas used for comparison were taken from the structure models obtained by Drits *et al.* (2010). The unit-cell atomic coordinates for $1M$ samples Mal-4 and Mal-6 (Supplementary Table S1) were calculated using the algorithm of Smoliar-Zviagina (1993), revised by Drits *et al.* (2010).

Results and discussion

Relationships between unit-cell parameters and cation composition

Layer-to-layer distance. The compositional variation from muscovite to aluminoceladonite through phengite is accompanied by a consistent decrease in the layer-to-layer distance, $c\sin\beta$. For group 1 samples, this decrease is nearly linear from muscovites ($c\sin\beta = 20.005$–19.930 Å) to phengites ($c\sin\beta = 19.896$–19.820
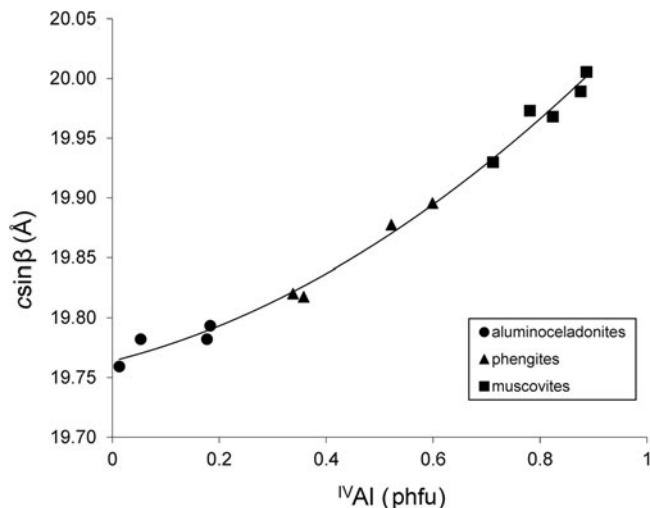
Fig. 1. Cross-plot of the $c\sin\beta$ values in group 1 samples against tetrahedral Al contents (cations phfu).

Fig. 2. Cross-plot of the $c\sin\beta$ values in the $1M$ K-dioctahedral micas and the $c\sin\beta/2$ values in group 1 and group 2 samples against tetrahedral Al contents (cations phfu).

Å) and then slows down from phengites to aluminoceladonites ($c\sin\beta$ = 19.793–19.759 Å) (Fig. 1), so that the dependence of $c\sin\beta$ on the contents of tetrahedral Al cations is described by the regression equation:

$$c\sin\beta = 19.766 + 0.280(^{IV}Al)^{1.5} \qquad (1)$$

(esd = 0.008 Å; R^2 = 0.993; $p < 10^{-12}$), where ^{IV}Al is the tetrahedral Al content.

In group 2 samples, a similar trend is observed, although the point scatter is much wider; the $c\sin\beta$ values for natural $2M_1$ micas plot onto or below the curve for synthetic $2M_1$ micas (Fig. 2). This may be associated with the more heterogeneous octahedral cation composition in natural mica samples, which, apart from Al and Mg, contain Fe, Mn, Cr, *etc*., as well as with the different methods of determination of unit-cell parameters (single-crystal X-ray, electron and neutron diffractions *vs* X-ray powder diffraction and Rietveld refinement used by Schmidt *et al.*, 2001).

The decrease in the $c\sin\beta$ parameter over the total composition range in natural and synthetic K-dioctahedral $2M_1$ and $3T$ micas, which belong to the solid-solution muscovite–aluminoceladonite, was previously noted by several authors (Massonne & Schreyer, 1986, 1989; Guidotti *et al.*, 1992; Ivaldi *et al.*, 2001; Schmidt *et al.*, 2001, Ferraris & Ivaldi, 2002), who explained it by a decrease in the tetrahedral rotation angle leading to increasing ditrigonal rings of the tetrahedral sheets across the interlayers, which allow the interlayer cation to 'sink' deeper into the interlayer cavity. Drits *et al.* (2010), however, showed that the mean interlayer distance, which determines the layer-to-layer distance value, depends primarily on Al-for-Si substitution. Decreasing tetrahedral Al-for-Si substitution leads to a decrease in the undersaturation of the basal oxygen atoms with respect to negative charge and, consequently, to weakening of their mutual repulsion. Accordingly, aluminoceladonites with little or no tetrahedral Al have shorter interlayer distances and, as a result, reduced $c\sin\beta$ values. The decrease in the interlayer distance with decreasing ^{IV}Al is balanced by a particular increase in the 2:1 layer thickness as a result of increasing octahedral sheet thickness with increasing contents of larger Mg (group 1) and Mg and Fe (group 2) cations
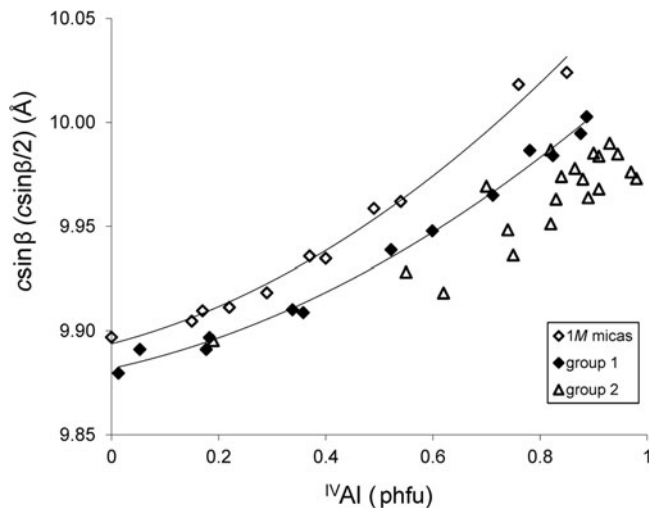
(Table 5), which probably explains the non-linear character of the dependence of $c\sin\beta$ on ^{IV}Al.

The dependence of $c\sin\beta$ on cation composition in natural and synthetic $2M_1$ micas of the muscovite–phengite–aluminoceladonite series is very similar to that observed in the low-temperature $1M$ micas in the series (Mg,Fe)-poor illite–Mg-rich illite–aluminoceladonite (Zviagina *et al.*, 2015):

$$c\sin\beta = 9.896 + 0.172(^{IV}Al)^{1.5} \qquad (2)$$

(esd = 0.004 Å; R^2 = 0.991, $p < 10^{-8}$). The respective trends are nearly parallel but the $c\sin\beta/2$ values of $2M_1$ micas of the muscovite–aluminoceladonite series are systematically lower than the $c\sin\beta$ values of natural $1M$ micas of the same tetrahedral composition (Fig. 2). This may be associated with the lower interlayer cation occupancy in the $1M$ micas ($\leq$0.8 cations phfu as compared to ~1 cations phfu in the $2M_1$ varieties). The presence of K cations in the interlayer cavities should partially compensate for the mutual repulsion between the basal oxygen anion planes across the interlayer, so that interlayer deficiency should lead, for the same tetrahedral cation compositions, to larger interlayer distances and therefore larger layer-to-layer distances. High-pressure formation conditions could be another reason for lower layer-to-layer distances in the $2M_1$ muscovite–phengite–aluminoceladonite micas as compared to those in the $1M$ illite–aluminoceladonite micas.

Layer displacement. With increasing Mg contents in the series of *tv* $1M$ illite–aluminoceladonite micas, the absolute value of the layer displacement $|c\cos\beta/a|$ decreases from ~0.40 in (Mg, Fe)-poor illite to ~0.36 in aluminoceladonite (Drits *et al.*, 2006; Zviagina *et al.*, 2015). Drits *et al.* (2006) showed that this effect is associated with the decreasing size difference between the occupied and vacant octahedra leading to $c\cos\beta/a$ values closer to the idealized value of –1/3. A similar trend is observed in the synthetic $2M_1$ micas (group 1) (Fig. 3). The relationships between $c\cos\beta/a$ and cation composition are described by Eq. 3 (Zviagina *et al.*, 2015) and Eq. 4 for the $1M$ micas and group 1, respectively:
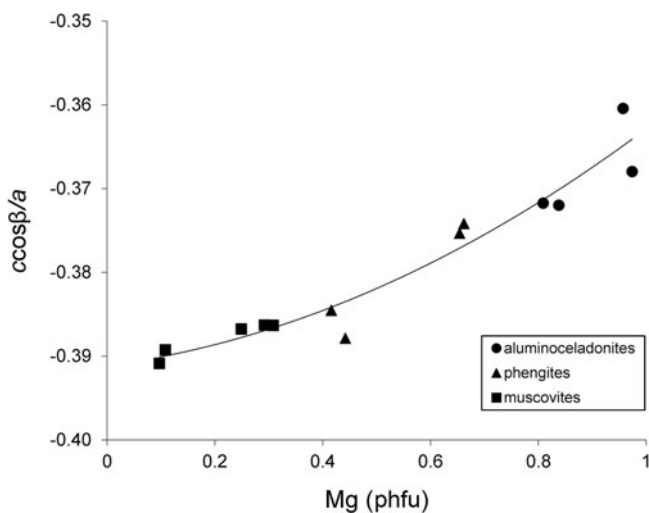
$$c\cos\beta/a = 0.084Mg^2 + 0.002Mg - 0.396 \qquad (3)$$

Table 5. Structure parameters in group 1 structure models and selected group 2 refined structures.[a]

Sample	Si	ΣR^{2+b}	(O–O)$_{basal}$ (Å)	(O–O)$_{lateral}$ (Å)	b_t/b_{oct}	α_{tet} (°)	<h_T> (Å)	<h_{oct}> (Å)	Δ_{OH} (Å)	<h_{TOT}> (Å)	<h_{int}> (Å)
					Group 1						
P13-1	3.987	0.974	2.607	2.878	1.046	2.7	2.221	2.188	0	6.628	3.252
P17	3.947	0.957	2.608	2.876	1.047	3.0	2.221	2.185	0	6.626	3.265
P11-2	3.823	0.838	2.610	2.869	1.050	4.4	2.220	2.167	0.007	6.613	3.278
P18-2	3.817	0.809	2.610	2.871	1.050	3.6	2.220	2.163	0.010	6.610	3.287
P12-1	3.662	0.662	2.620	2.856	1.059	5.3	2.226	2.143	0.021	6.608	3.302
P15	3.642	0.654	2.622	2.856	1.060	5.6	2.226	2.142	0.021	6.607	3.302
P28	3.478	0.416	2.630	2.835	1.071	7.5	2.224	2.115	0.039	6.590	3.348
P25	3.401	0.442	2.635	2.837	1.073	8.1	2.225	2.118	0.037	6.592	3.356
P33	3.288	0.308	2.641	2.823	1.080	9.1	2.224	2.105	0.048	6.585	3.380
P30	3.219	0.249	2.645	2.817	1.084	9.9	2.224	2.101	0.052	6.583	3.404
P26	3.176	0.292	2.648	2.821	1.084	10.0	2.224	2.104	0.049	6.584	3.400
P31	3.124	0.108	2.652	2.808	1.091	11.2	2.223	2.093	0.063	6.580	3.414
P29	3.113	0.887	2.653	2.799	1.094	11.2	2.223	2.092	0.064	6.580	3.422
					Group 2						
19	3.81	0.79	2.610	2.861	1.053	2.4	2.220	2.164	0.003	6.607	3.288
18	3.45	0.57	2.628	2.851	1.064	5.2	2.229	2.130	0.028	6.606	3.321
17	3.38	0.45	2.629	2.842	1.069	6.3	2.226	2.118	0.034	6.593	3.325
16	3.25	0.42	2.639	2.838	1.074	7.9	2.222	2.121	0.044	6.594	3.342
6	3.11	0.12	2.658	2.808	1.093	11.4	2.229	2.095	0.062	6.594	3.370
9	3.03	0.13	2.656	2.807	1.092	11.2	2.223	2.086	0.066	6.572	3.404

[a] Sample numbers as in Table 3.
[b] ΣR^{2+} = Mg for group 1.
(O–O)$_{basal}$ = tetrahedral basal edge length; (O–O)$_{lateral}$ = octahedral lateral edge length; b_t/b_{oct} = tetrahedral/octahedral misfit; α_{tet} = tetrahedral rotation angle; <h_T> = mean tetrahedral sheet thickness; <h_{oct}> = mean octahedral sheet thickness; Δ_{OH} = corrugation of the octahedral basal anion surface (hydroxyl depression); <h_{TOT}> = 2 <h_T> + <h_{oct}> + 2Δ_{OH}/3 = mean thickness of the 2:1 layer; <h_{int}> = mean interlayer distance.

Fig. 3. Cross-plot of the $c\cos\beta/a$ values in group 1 samples against Mg contents (cations phfu).

Fig. 4. Cross-plot of the $c\cos\beta/a$ values in group 2 samples against Mg contents (cations phfu).
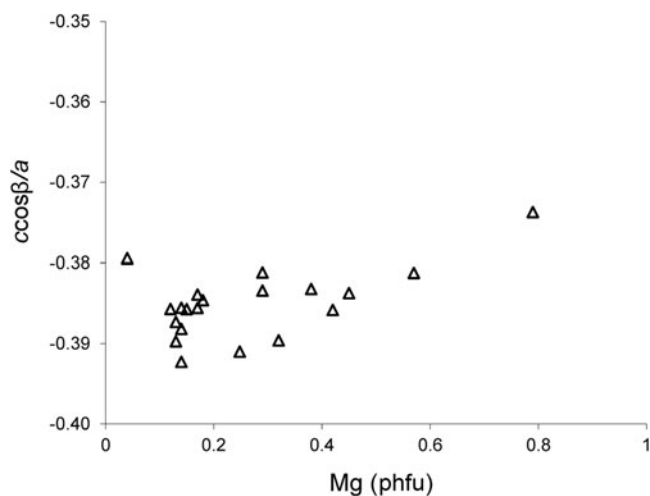
(esd = 0.005; R^2 = 0.888; $p < 10^{-4}$), and:

$$c\cos\beta/a = 0.020Mg^2 + 0.008Mg - 0.391 \quad (4)$$

(esd = 0.002; R^2 = 0.937; $p < 10^{-7}$). For group 1, the relationship between $c\cos\beta/a$ and Mg can be described by a linear function:

$$c\cos\beta/a = 0.030Mg - 0.395 \quad (4a)$$

with only slightly less precision (esd = 0.003; R^2 = 0.915; $p < 10^{-6}$). The refined structures (group 2) display a similar but fairly loose trend with a much wider point scatter (Fig. 4): the |$c\cos\beta/a$|

values are 0.38–0.39 for muscovites and phengites and ~0.37 for aluminoceladonite. Similarly to the $c\sin\beta$ values, the wide scatter of points is associated with the more heterogeneous cation composition of the group 2 samples, which contain other octahedral cations (Fe, Mn, Cr, *etc.*) in addition to Al and Mg, as well as with the different methods of determination of unit-cell parameters (see above).

Lateral dimensions. Schmidt *et al.* (2001) noted that the *a* and *b* parameters of their synthetic samples increased from muscovites to phengites having ^{IV}Al ≈ 0.4 and Mg ≈ 0.6 cations phfu and decreased from phengites to aluminoceladonites. However, no quantitative treatment of this trend was provided. Regression
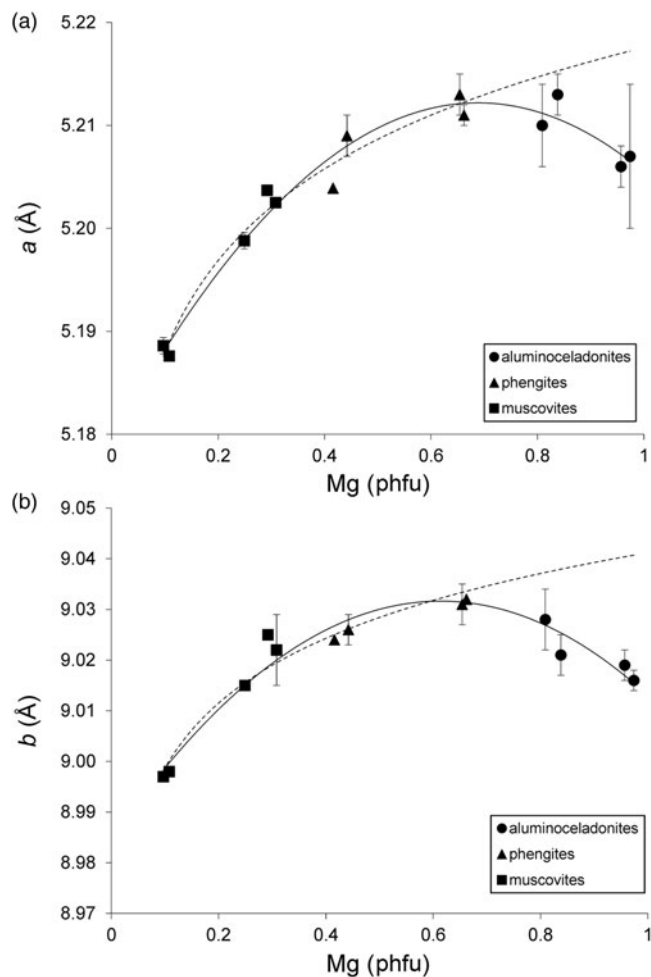
Fig. 5. Cross-plot of the (a) *a* and (b) *b* values in group 1 samples against Mg contents (cations phfu). Solid line = actual trend; dotted line = extrapolation of the dependences observed in the series muscovite–phengite to aluminoceladonite composition. Error bars: experimental *esd* values for (a) *a* and (b) *b* (*esd* values ≤ 0.0008 Å for *a* and ≤ 0.001 Å for *b* are not displayed).

analysis of the *a* and *b* values in group 1 samples yields the following relationships:

$$a = -0.069(\text{Mg} - 0.688)^2 + 5.212 \qquad (5)$$

($esd = 0.002$ Å; $R^2 = 0.964$; $p < 10^{-7}$) (Fig. 5a), and:

$$b = -0.125(\text{Mg} - 0.614)^2 + 9.032 \qquad (6)$$

($esd = 0.003$ Å; $R^2 = 0.942$; $p < 10^{-6}$) (Fig. 5b). Equations 5 and 6 show that the reversal of the trend in the variation of the *a* and *b* parameters indeed takes place at Mg = 0.6–0.7 cations phfu. The trends in the variation of the lateral cell dimensions with cation composition in group 2 samples are similar to those in group 1 samples, but the point scatter is wider (Fig. 6) and the correlations are not as strong. As hypothesized for *c*sinβ, this may be associated with the presence of octahedral cations other than Al and Mg (in the first place, Fe^{2+} and Fe^{3+}), as well as with differences in unit-cell determination techniques. Specifically, the *b* parameter increases from ∼8.98–9.03 Å in muscovites to ∼9.05 Å in phengites and then decreases to 9.037 Å in aluminoceladonite (Fig. 6, Table 4).
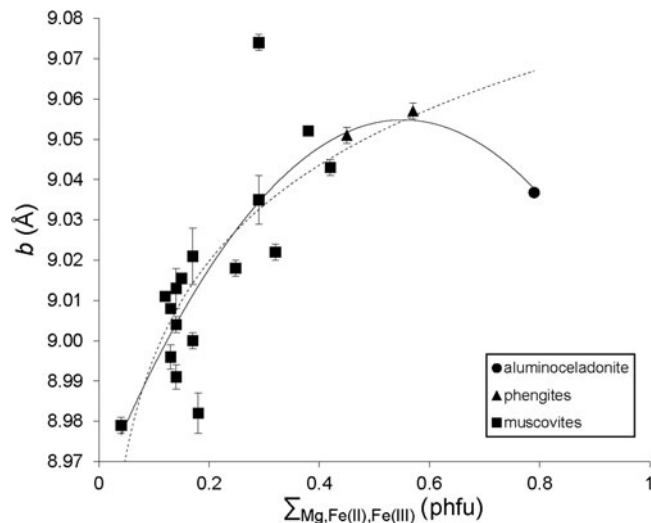

Fig. 6. Cross-plot of the *b* values in group 2 samples against total amount of Mg, Fe^{2+} and Fe^{3+} (cations phfu). Solid line = actual trend; dotted line = extrapolation of the dependence observed in the series muscovite–phengite to aluminoceladonite composition. Error bars: experimental *esd* values for *b* (*esd* values ≤ 0.001 Å are not displayed).

This trend can be described by a regression similar to Eq. 6 but with lower statistical significance:

$$b = 9.055 - 0.299(\Sigma_{\text{Mg,Fe(II),Fe(III)}} - 0.551)^2 \qquad (7a)$$

($esd = 0.015$ Å; $R^2 = 0.70$; $p < 10^{-4}$), where $\Sigma_{\text{Mg,Fe(II),Fe(III)}}$ is the total amount of Mg, Fe^{2+} and Fe^{3+} cations phfu. Equation 7a shows that the maximum *b* value is achieved for the sum of Mg and Fe of ∼0.55 cations phfu. If the same trend is analysed without including the data on the only aluminoceladonite sample in group 2, a very similar equation is obtained:

$$b = 9.050 - 0.292(\Sigma_{\text{Mg,Fe(II),Fe(III)}} - 0.538)^2 \qquad (7b)$$

($esd = 0.015$ Å; $R^2 = 0.68$; $p < 10^{-4}$). For $2M_1$ aluminoceladonite (Smyth *et al.*, 2000), Eq. 7b predicts $b = 9.028$ Å, which is less than 0.01 Å lower than the observed *b* value (9.037 Å) and is identical to that of sample P18-2 (group 1) of similar cation composition.

A similar trend was reported for $1M$ Al-rich, K-dioctahedral micas. In the illite–aluminoceladonite series, *b* increases from ∼9 Å in (Mg,Fe)-poor illites up to ∼9.03–9.04 Å in Mg-rich illites and then decreases to ∼9.01–9.02 Å in aluminoceladonites, so that:

$$b = 9.039 - 0.121(\text{Mg} - 0.287)^2 - 0.689(Fe^{2+} - 0.116)^2$$
$$- 1.994(Fe^{3+} - 0.154)^2 \qquad (8)$$

($esd = 0.006$ Å; $R^2 = 0.963$, $p = 0.008$) (Zviagina *et al.*, 2015).

Schmidt *et al.* (2001) suggested that the reduction of *a* and *b* cell parameters 'at high aluminoceladonite contents' (*i.e.* for Si > 3.6 and Mg > 0.6 cations phfu) could be associated with a possible partial trioctahedral character of aluminoceladonite-like micas. This hypothesis, however, is not convincing, as according to the crystal-chemical formulae the occupancies of the *trans*-octahedron are negligible (Tables 1; Tables 2, sample #19). A more plausible explanation is based on the analysis of the

evolution of tetrahedral and octahedral edge lengths and sheet thicknesses. The actual lateral dimensions of the mica structure can be seen as a compromise between the larger dimensions of the idealized unrotated tetrahedral sheet and the smaller dimensions of the idealized octahedral sheet, b_t and b_{oct}, which are related to the mean tetrahedral basal and octahedral unshared lateral edge lengths, $(O–O)_{basal}$ and $(O–O)_{lateral}$, respectively, by: $b_t = 2\sqrt{3}(O–O)_{basal}$; $b_{oct} = 3(O–O)_{lateral}$. With increasing Si contents, the tetrahedral size decreases while tetrahedral elongation increases (Drits *et al.*, 2010; Zviagina & Drits, 2012), and, as a result, $(O–O)_{basal}$ decreases. Simultaneously, increasing contents of larger octahedral cations (Mg, Fe^{2+}, Fe^{3+}) lead to increasing $(O–O)_{lateral}$ values (Table 5). In both muscovite–phengite and (Mg,Fe)-poor illite–Mg-rich illite series, the second of these trends dominates and b increases; from phengite to $2M_1$ aluminoceladonite, as well as from Mg-rich illite to $1M$ aluminoceladonite, the decrease in $(O–O)_{basal}$ begins to dominate and b decreases. The a parameter behaves in a similar way. The change of the trends in question may be associated with a decrease in mutual repulsion of octahedral cations with increasing contents of divalent cations. As a result, the octahedral sheet becomes less flattened and its lateral dimensions increase more slowly. Accordingly, the decreasing lateral dimensions of the tetrahedral sheet begin to dominate.

On the whole, the variation of the b parameter with b_t/b_{oct} can be described by regression Eqs. 9a and 9b for group 1 and group 2 samples, respectively;

$$b = 9.031 - 39.330(b_t/b_{oct} - 1.064)^2 \qquad (9a)$$

$(esd = 0.004$ Å, $R^2 = 0.869$, $p < 10^{-4})$ (Fig. 7), and:

$$b = 9.059 - 94.019(b_t/b_{oct} - 1.069)^2 \qquad (9b)$$

$(esd = 0.009$ Å, $R^2 = 0.864$, $p < 10^{-8})$ (Fig. 8). For regressions (9a) and (9b), the b_t/b_{oct} values were obtained from structural models and from experimental $(O–O)_{basal}$ and $(O–O)_{lateral}$ values, respectively (Table 5).

For $1M$ micas in the illite–aluminoceladonite series, the correlation between the b parameters and b_t/b_{oct} values is weaker and displays a wider scatter of points than in the case of $2M_1$ micas (Fig. 9) (the b_t and b_{oct} parameters (Table 6) were calculated using the structure modelling algorithm for $1M$ dioctahedral micas of Smoliar-Zviagina (1993) and Drits *et al.* (2010)). This may be associated with the higher structural and crystal-chemical heterogeneity of the low-temperature micas and, in particular, interlayer cation deficiency and the presence of expandable interlayers, the higher Fe contents in some samples, the high dispersion and the lower structural order. The general trend, however, is similar: with increasing contents of tetrahedral Si and larger octahedral cations, b increases up to Mg ≈ 0.4 cations phfu and then decreases (Fig. 10). The similar trends in the variations of the unit-cell parameters (layer-to-layer distance, layer displacement and lateral dimensions) with cation composition observed in $2M_1$ Al-rich, K-dioctahedral micas and in $1M$ micas of the illite–aluminoceladonite series suggest that these variations should be controlled by similar structural factors.
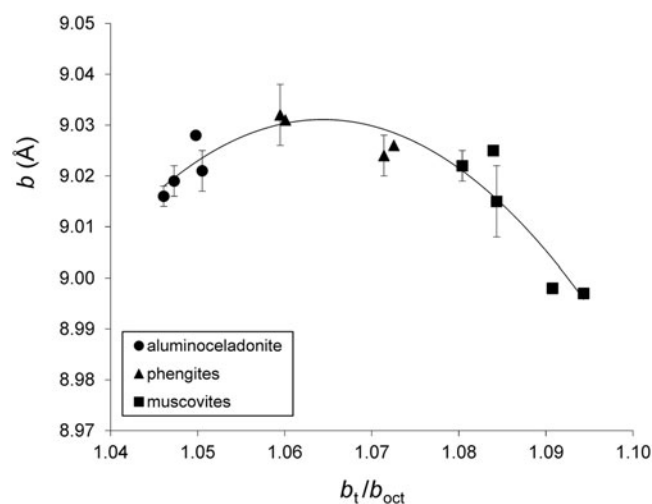

Fig. 7. Cross-plot of the b values in group 1 samples against b_t/b_{oct} (see text for explanation). Error bars: experimental *esd* values for b (*esd* values ≤0.001 Å are not displayed).
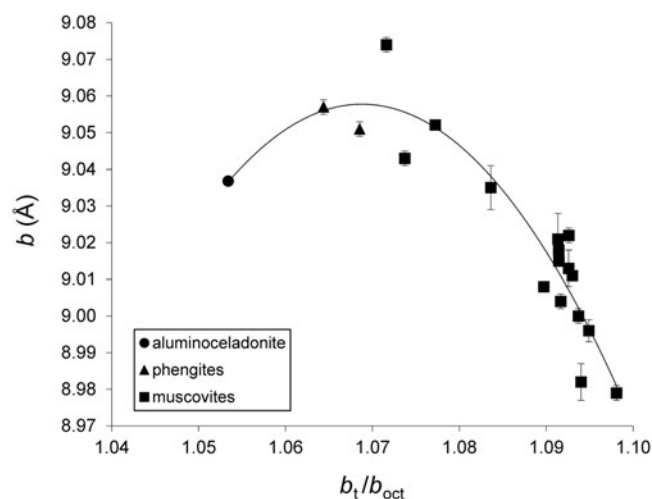

Fig. 8. Cross-plot of the b values in group 2 samples against b_t/b_{oct} (see text for explanation). Error bars: experimental *esd* values for b (*esd* values ≤ 0.001 Å are not displayed).

Tetrahedral rotation angle and interlayer structure

In agreement with the estimates of Schmidt *et al.* (2001), the calculated ditrigonal tetrahedral rotation angle values, α_{tet}, decrease from muscovite to aluminoceladonite. The α_{tet} values are ~3–4° for aluminoceladonite, ~5–8° for phengite and ~9–11° for muscovite structure models (group 1, Table 5). The decrease in α_{tet} is associated with a decrease in the tetrahedral basal edge lengths with increasing Si and can be described by the empirical relationship $\alpha_{tet} = arccos\left(\dfrac{0.8672b}{3(O-O)basal}\right)$ (Zviagina & Drits, 2012). The modelled α_{tet} values are lower than those predicted for the same samples by Schmidt *et al.* (2001) based on the empirical relationship of Radoslovich & Norrish (1962) (~5–7° for aluminoceladonites, ~9–11° for phengites and ~12–15° for muscovites), but agree well with the observed α_{tet} values in refined mica structures of respective compositions: aluminoceladonite, 2.4°; phengites and phengitic muscovite, ~5–8°; and muscovite, ~11° (group 2,
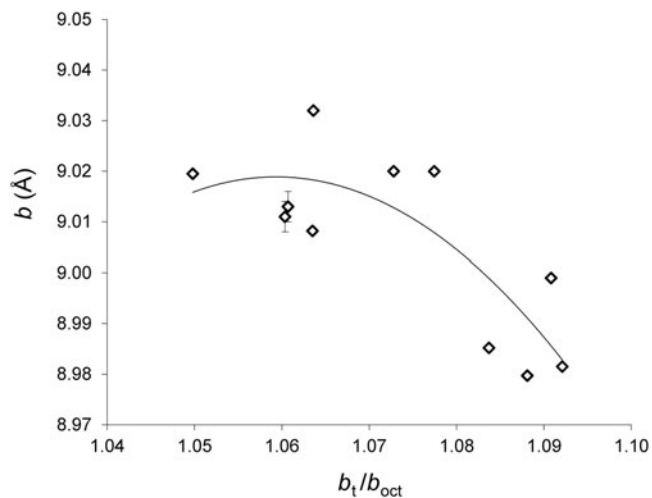
Fig. 9. Cross-plot of the *b* values in the 1*M* K-dioctahedral micas against b_t/b_{oct} (see text for explanation). Error bars: experimental *esd* values for *b* (*esd* values ≤ 0.001 Å are not displayed).

Table 6. Tetrahedral basal and octahedral lateral edge lengths, tetrahedral/octahedral lateral misfit values and tetrahedral rotation angles in 1*M* mica structure models.[a]

Sample	Si	ΣR^{2+}	(O–O)$_{basal}$ (Å)	(O–O)$_{lateral}$ (Å)	b_t/b_{oct}[b]	α_{tet} (°)
M422	3.15	0.05	2.652	2.804	1.092	11.1
RM30	3.24	0.13	2.647	2.809	1.088	10.6
10564	3.27	0.15	2.647	2.802	1.091	10.6
Zempleni	3.36	0.16	2.641	2.814	1.083	9.8
Silver Hill	3.46	0.29	2.636	2.825	1.077	8.5
KJMC3	3.51	0.43	2.633	2.834	1.073	8.2
60/3	3.63	0.56	2.627	2.850	1.063	5.7
602/1	3.71	0.60	2.624	2.849	1.064	6.7
Mal-4	3.83	0.54	2.619	2.852	1.060	4.3
Mal-6	3.86	0.60	2.618	2.850	1.060	5.3
136	4.00	0.79	2.612	2.873	1.050	3.0

[a] Cation compositions of 1*M* micas: Drits *et al.* (2010), Zviagina *et al.* (2015). 1*M* structure models: Mal-4 and Mal-6 from this work; other samples from Drits *et al.* (2010).
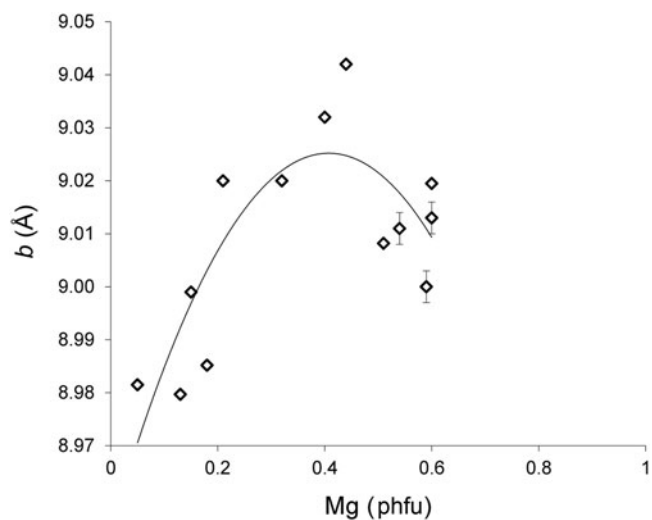[b] $b_t/b_{oct} = 2\sqrt{3}(O–O)_{basal}/3(O–O)_{lateral}$.

Fig. 10. Cross-plot of the *b* values in the 1*M* K-dioctahedral micas against Mg contents (cations phfu). Error bars: experimental *esd* values for *b* (*esd* values ≤ 0.001 Å are not displayed).

Table 5). The decrease in α_{tet} values leads to a decrease in the differences between the mean inner and outer K–O distances (<K–O>$_{in}$ and <K–O>$_{out}$) and, at the same time, to an increase in the individual and mean inner K–O distances (Table 7). The longer inner K–O distances imply weaker bonding between the interlayer cation and the basal oxygen anions, therefore leading to a less stable interlayer configuration.

The α_{tet} values obtained for the structure models of 1*M* aluminoceladonites are close to those for the 2*M*$_1$ structures of similar tetrahedral composition: 3–5° for aluminoceladonites, 6–8° for Mg-rich illites and 10–11° for (Mg,Fe)-poor illites (Table 6).

Along with the decrease in α_{tet} values and the increase in inner K–O distances, the increasing contents of Si and Mg (R^{2+}) lead to a decrease in the tetrahedral basal anion surface corrugation (tetrahedral tilt), as well as in the O–O distances across the interlayer (Table 8). Comparison of the interlayer structure in selected 2*M*$_1$ and 1*M* structures (Table 8) shows that 1*M* micas tend to have longer mean O–O distances across the interlayer and larger interlayer distances, <h_{int}>, than those for 2*M*$_1$ varieties of similar cation compositions. The distribution of individual anion–anion distances in the interlayer in *tv* 2*M*$_1$ mica structures is similar to those in *cv* 1*M* structures, but differs from those in *tv* 1*M* structures because of a different mutual arrangement of depressed (O*) and non-depressed (O) basal oxygen anions in the tetrahedral sheets across the interlayer (Fig. 11). A 2*M*$_1$ structure has two longer O–O* distances and one shorter O–O distance, whereas in a 1*M* structure, there are two shorter O–O distances and one longer O*–O* distance (Table 8). At the same time, the shorter O–O distances in 1*M* micas are still longer than the shorter O–O distances in 2*M*$_1$ micas of similar composition because of shorter interlayer distances, possibly due to higher occupancy of the interlayer site. For aluminoceladonite-like varieties having the shortest O–O distance, this could favour the occurrence of the 1*M* structure as compared to the 2*M*$_1$ polytype.

Structure models with extrapolated unit-cell parameters

To elucidate the possible structural factors leading to a reduction of lateral dimensions from phengite to aluminoceladonite, the dependences of *a* and *b* parameters on Mg contents observed in the series of synthetic muscovite–phengite samples (group 1) were extrapolated to aluminoceladoite composition, and aluminoceladonite structures were modelled using the extrapolated *a* and *b* cell parameters. The increase in *a* and *b* from muscovites to phengites can be approximated as:

$$a = 5.218 + 0.013 \ln(Mg) \quad (11)$$

(*esd* = 0.002 Å; R^2 = 0.970; $p < 10^{-5}$) (Fig. 5a, dotted line), and:

$$b = 9.041 + 0.018 \ln(Mg) \quad (12)$$

(*esd* = 0.003 Å; R^2 = 0.953; $p < 10^{-5}$) (Fig. 5b, dotted line). For aluminoceladonite samples with Mg approaching 1 cation phfu (samples P13-1. P17, P11-2 and P18-2, Mg = 0.81-0.97 cations phfu), Eqs. 11 and 12 predict *a* = 5.215–5.218 Å and *b* ≈ 9.04 Å instead of the observed values of 5.20–5.21 Å and 9.016–9.028 Å, respectively. Attempts to model the structures of Si-rich (Si ≈ 4 cations phfu) synthetic micas (samples P13-1 and P17) using extrapolated *a* and *b* cell parameters show that the models (P13-1e and P17e, Supplementary Table S1) can only be realized with α_{tet} forced to 0° and additional distortions of the tetrahedra, such as additional

Table 7. K–O distances (Å) in selected structure models (group 1) and refined structures (group 2).[a]

Sample	Si	ΣR^{2+b}	α_{tet} (°)	Inner				Outer				<K–O>	Δ<K–O>
				K–O3	K–O4	K–O5	<K–O>$_{in}$	K–O3	K–O4	K–O5	<K–O>$_{out}$		
							Group 1						
P13-1	3.987	0.974	2.7	3.003	3.031	2.996	3.010	3.097	3.188	3.103	3.129	3.070	0.119
P13-1e	3.987	0.974	0	3.057	3.094	3.062	3.071	3.052	3.134	3.049	3.078	3.075	0.007
P17	3.947	0.957	3.0	2.990	3.030	3.004	3.008	3.115	3.200	3.102	3.139	3.073	0.131
P17e	3.947	0.957	0	3.052	3.098	3.075	3.075	3.063	3.139	3.041	3.081	3.078	0.006
P18-2	3.817	0.809	3.6	2.989	3.023	2.989	3.001	3.125	3.235	3.127	3.162	3.082	0.162
P15	3.642	0.654	5.6	2.951	2.984	2.956	2.964	3.169	3.300	3.164	3.211	3.087	0.247
P28	3.478	0.416	7.5	2.919	2.951	2.924	2.931	3.209	3.380	3.207	3.265	3.098	0.334
P33	3.288	0.308	9.1	2.890	2.926	2.900	2.905	3.249	3.436	3.243	3.310	3.107	0.404
P29	3.113	0.887	11.2	2.850	2.889	2.864	2.868	3.293	3.513	3.281	3.362	3.115	0.494
							Group 2						
19	3.81	0.79	2.4	3.015	3.055	3.018	3.029	3.100	3.205	3.100	3.135	3.082	0.106
18	3.45	0.57	5.2	2.972	3.005	2.973	2.983	3.168	3.310	3.161	3.213	3.098	0.230
17	3.38	0.45	6.3	2.944	2.978	2.948	2.957	3.185	3.342	3.180	3.236	3.096	0.279
16	3.25	0.42	7.9	2.911	2.948	2.918	2.925	3.223	3.397	3.216	3.279	3.102	0.354
6	3.11	0.12	11.4	2.833	2.867	2.845	2.848	3.292	3.507	3.274	3.358	3.103	0.510
9	3.03	0.13	11.2	2.848	2.883	2.860	2.864	3.294	3.514	3.278	3.362	3.113	0.498

[a] Sample numbers as in Table 3.
[b] ΣR^{2+} = Mg for group 1.
α_{tet} = tetrahedral rotation angle; <K–O>$_{in}$ = mean inner K–O distance; <K–O>$_{out}$ = mean outer K–O distance; <K–O> = mean total K–O distance; Δ<K–O> = <K–O>$_{out}$ – <K–O>$_{in}$.

Table 8. Typical characteristics of the interlayer in $2M_1$ refined structures,[a] a $2M_1$ aluminoceladonite structure model[b] and $1M$ structure models.[c]

| Sample	Si	ΣR^{2+}	Anion–anion across interlayer (Å)			<h_{int}> (Å)	h_{imin} (Å)	ΔZ (Å)
			Short	Long	Mean			
RM30	3.24	0.05	3.340(×2)	3.819	3.500	3.452	3.306	0.219
#12	3.18	0.24	3.300	3.510(×2)	3.440	3.393	3.260	0.217
KJMC3	3.51	0.43	3.289(×2)	3.663	3.414	3.385	3.268	0.174
#18	3.45	0.57	3.229	3.383(×2)	3.332	3.320	3.221	0.161
Mal-6	3.85	0.60	3.241(×2)	3.564	3.349	3.337	3.233	0.156
#19	3.81	0.79	3.212	3.332(×2)	3.292	3.289	3.210	0.133
136	4.00	0.79	3.223(×2)	3.489	3.312	3.308	3.220	0.131
P13-1	4.00	0.97	3.166	3.281(×2)	3.243	3.240	3.165	0.112

[a] #12 = muscovite; #18 = phengite; #19 = aluminoceladonite; sample numbers as in Table 3.
[b] P13-1 = $2M_1$ aluminoceladonite structure model.
[c] RM30, KJMC3 = illites; Mal-6, 136 = aluninoceladonites; sample names for $1M$ micas are in italics.
<h_{int}> = mean interlayer distance; h_{imin} = interlayer distance calculated over non-depressed basal oxygen anions; ΔZ = tetrahedral tilt.

elongation of the bridging bonds T1–O3 and T2–O5 (1.645(5) Å and 1.642(7) Å, as compared to 1.641(5) Å and 1.635(7) Å, respectively, for the structure models based on the observed unit-cell parameters with $\alpha_{tet} \approx 3°$). Moreover, forcing α_{tet} to 0° leads to a redistribution of individual K–O bond lengths, leading to further minimization of the difference between the inner and outer K–O distances and further increases in the inner K–O distances (Table 7). As a result, the interlayer configuration, as well as the structure as a whole, should become less stable.

In group 2 micas, the increase in the *b* parameter from muscovites to phengites can be approximated as:

$$b = 9.075 + 0.134 \ln(Mg) \qquad (13)$$

($R^2 = 0.66$) (Fig. 6, dotted line), which would predict $b = 9.067$ Å and 9.075 Å for Mg = 0.8 and 1 cations phfu, respectively. Obviously, such extremely large lateral dimensions in a mica with aluminoceladonite-like composition would require zero
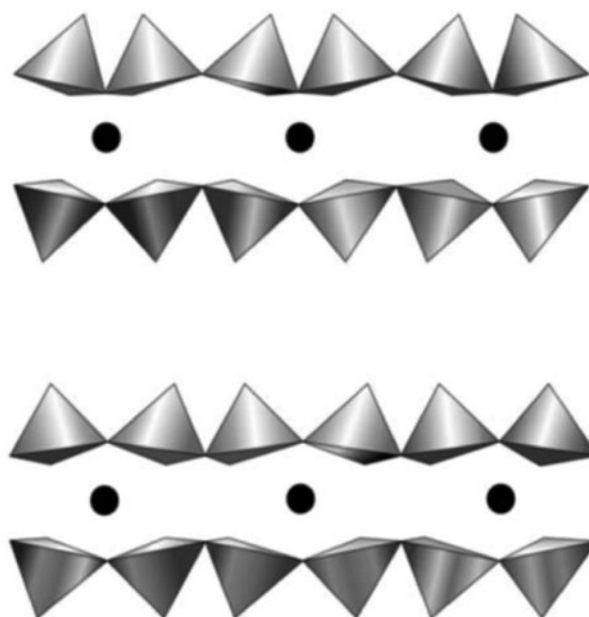
Fig. 11. Comparison of interlayer cavities in *tv* $2M_1$ (upper) and $1M$ (lower) structures. In contrast to the $1M$ structure, distances between the nearest depressed and non-depressed basal oxygens atoms across the interlayer in the $2M_1$ structure are partially equalized (see text for explanation) (modified after Drits *et al.*, 2006).

tetrahedral rotation, leading to structural effects similar to those in the P13-1e and P17e structure models.

Therefore, ensuring a larger α_{tet} in order to stabilize the structure may serve, along with tetrahedral elongation and tetrahedral size reduction, as an additional factor leading to a decrease in the lateral dimensions.

Conclusion

The similarities in the variations of unit-cell parameters with cation composition observed in $2M_1$ and $1M$ natural and synthetic

K-dioctahedral micas imply that these variations should be controlled by similar structural factors. These factors, which are related to the ability of tetrahedral and octahedral sheets having different lateral dimensions to form a layer with uniform two-dimensional periodicity, are realized in a different manner in micas formed under different pressure and temperature conditions; that is, these structural factors are similar but not identical. Extremely high temperatures and pressures in a closed system under laboratory conditions allow structural readjustment of the differently sized tetrahedral and octahedral sheets for a wide range of cation compositions (from muscovite to aluminoceladonite through phengite). In nature, under the conditions of metamorphism, the temperatures and pressures are not high enough to enable this readjustment for the formation of micas with aluminoceladonite-like compositions, which, in particular, would require reductions of the a and b parameters to ensure higher tetrahedral rotation. Therefore, under high-pressure metamorphic conditions in Mg-rich environments, phengites are frequently formed in association with chlorites, which accumulate high quantities of Mg cations (Vidal & Parra, 2000, and references therein).

Unlike muscovites and phengites, micas in the illite–aluminoceladonite series are formed under low-temperature and low-pressure non-equilibrium conditions in systems with highly heterogeneous compositions. This suggests that, along with the structure, other factors might have a significant effect on the occurrence of $1M$ aluminoceladonite. At the same time, the readjustment of the lateral dimensions of tetrahedral and octahedral sheets in $1M$ K-dioctahedral micas may be facilitated by the more heterogeneous composition of the environment, leading to a wide range of cation compositions. Additional factors that could favour the occurrence of the $1M$ aluminoceladonite structure as compared to the $2M_1$ polytype could be the relatively longer O–O distances across the interlayer and the relatively higher $<h_{int}>$ values.

References

Bailey S.W. (1984) Crystal chemistry of the true mica. Pp. 13–60 in: *Micas* (S.W. Bailey, editor), Reviews in Mineralogy, **13**. Mineralogical Society of America, Washington, DC, USA.

Beyer S.R., Kyser K., Hiatt E.E. & Fraser I. (2010) Geological evolution and exploration geochemistry of the Boomerang Lake unconformity-type uranium prospect, Northwest Territories, Canada. *Society of Economic Geologists, Special Publication*, **15**, 675–702.

Brigatti M.F. & Guggenheim S. (2002) Mica crystal chemistry and the influence of pressure, temperature and solid solution on atomistic models. Pp. 1–97 in: *Micas: Crystal Chemistry and Metamorphic Petrology* (A. Mottana, F.E. Sassi, J.B. Thompson Jr & S. Guggenheim, editors). Reviews in Mineralogy and Geochemistry, **46**. Mineralogical Society of America, Washington, DC, USA, with Accademia Nazionale dei Lincei, Rome, Italy.

Brigatti M.F., Frigieri P. & Poppi L. (1998) Crystal chemistry of Mg-, Fe^{2+}-bearing muscovites-$2M_1$. *American Mineralogist*, **83**, 775–785.

Brigatti M.F., Galli E., Medici L., Poppi L., Cibin G., Marcelli A. & Mottana A. (2001) Chromium-containing muscovite: crystal chemistry and XANES spectroscopy. *European Journal of Mineralogy*, **13**, 377–389.

Curetti N., Ferraris G. & Ivaldi G. (2008) Correlation between crystallization pressure and structural parameters of phengites. *American Mineralogist*, **93**, 451–455.

Domanik K. & Holloway J.R. (1996) The stability and composition of phengitic muscovite and associated phases from 5.5 to 11 GPa: implications for deeply subducted sediments. *Geochimica et Cosmochimica Acta*, **60**, 4133–4150.

Drits V.A. & Kossovskaya A.G. (1991) *Clay Minerals: Micas and Chlorites*. Nauka, Moscow, Russia, 175 pp. (in Russian).

Drits V.A., McCarty D.K. & Zviagina B.B. (2006) Crystal-chemical factors responsible for the distribution of octahedral cations over *trans*- and *cis*-sites in dioctahedral 2:1 layer silicates. *Clays and Clay Minerals*, **54**, 131–153.

Drits V.A., Zviagina B.B., McCarty D.K. & Salyn A.L. (2010) Factors responsible for crystal-chemical variations in the solid solutions from illite to aluminoceladonite and from glauconite to celadonite. *American Mineralogist*, **95**, 348–361.

Ferraris G. and Ivaldi G. (2002) Structural features of micas. Pp. 117–153 in: *Micas: Crystal Chemistry and Metamorphic Petrology* (A. Mottana, F.E. Sassi, J.B. Thompson Jr & S. Guggenheim, editors). Reviews in Mineralogy and Geochemistry, **46**. Mineralogical Society of America, Washington, DC, USA, with Accademia Nazionale dei Lincei, Rome, Italy.

Guggenheim S., Chang Y.H. & Koster van Groos A.F. (1987) Muscovite dehydroxylation: high-temperature studies. *American Mineralogist*, **72**, 537–550.

Guidotti C.V., Mazzoli C., Sassi F.P. & Blencoe J.G. (1992) Compositional controls on the cell dimensions of $2M_1$ muscovite and paragonite. *European Journal of Mineralogy*, **4**, 283–297.

Güven N. (1971) The crystal structures of $2M_1$ phengite and $2M_1$ muscovite. *Zeitschrift für Kristallographie*, **134**, 196–212.

Ivaldi G., Ferraris G., Curetti N. & Compagnoni R. (2001) Coexisting $3T$ and $2M_1$ polytypes in a phengite from Cima Pal (Val Savenca, western Alps): chemical and polytypic zoning and structural characterization. *European Journal of Mineralogy*, **13**, 1025–1034.

Knurr R.A. & Bailey S.W. (1986) Refinement of Mn-substituted muscovite and phlogopite. *Clays and Clay Minerals*, **34**, 7–16.

Massonne H.J. & Schreyer W. (1986) High-pressure syntheses and X-ray properties of white micas in the system K$_2$O–MgO–Al$_2$O$_3$–SiO$_2$–H$_2$O. *Neues Jahrbuch Mineralogie Abhandlungen*, **153**, 177–215.

Murao R., Yubuta K., Miyawaki R. & Sugiyama K. (2009) Analysis of aluminoceladonite included in green heulandite. *JAKOKA: 2009 Annual Meeting of the Japan Association of Mineralogical Sciences*, abs. R4-11, p. 105.

Pavese A., Ferraris G., Pischedda V. & Ibberson R. (1999) Tetrahedral order in phengite $2M_1$ upon heating, from powder neutron diffraction, and thermodynamic consequences. *European Journal of Mineralogy*, **11**, 309–320.

Pe-Piper G. (1985) Dioctahedral micas in Triassic metavolcanic rocks of western Greece. *Canadian Mineralogist*, **23**, 597–608.

Petrova V.V. & Amarjargal P. (1996) *Zeolites of Mongolia*. Nauka, Moscow, Russia, 150 pp. (in Russian).

Radoslovich E.W. & Norrish K. (1962) The cell dimensions and symmetry of layer–lattice silicates. Some structural considerations. *American Mineralogist*, **47**, 599–616.

Rasskazov A.A. (1984) *Clay Minerals of Potassium-Bearing Deposits (Area of Starobinsky Deposit)*. Nauka, Moscow, Russia, 72 pp. (in Russian).

Rieder M., Cavazzini G., D'yakonov Y.S., Frank-Kamenetskii V.A., Gottardi G., Guggenheim S., Koval P.V., Muller G., Neiva A.M.R., Radoslovich E.W., Robert J.-L., Sassi F.P., Takeda H., Weiss Z. & Wones D.R. (1998) Nomenclature of the micas. *Clays and Clay Minerals*, **46**, 586–595.

Ripp G.S., Doroshkevich A.G., Karmanov N.S. & Kanakin S. V. (2009) Micas from the Khaluta carbonatite deposit, Western Transbaikal Region. *Geology of Ore Deposits*, **51**, 812–821.

Rothbauer R. (1971) Untersuchung eines $2M_1$-muskovits mit neutronenstrahlen. *Neues Jahrbuch für Mineralogie Monatshefte*, **44**, 143–154.

Rule A.C. & Bailey S.W. (1985) Refinement of the crystal structure of phengite-$2M_1$. *Clays and Clay Minerals*, **33**, 403–409.

Sassi F.P., Guidotti C.V., Reider M. & de Pieri R. (1994) On the occurrence of metamorphic $2M1$ phengite: some thoughts on polytypism and crystallization conditions of $3T$ phengites. *European Journal of Mineralogy*, **6**, 171–178.

Sassi R., Brigatti M.F., Gomez-Pugnaire M.T., Peruzzo L., Tellini F. & Sassi F.P. (2010) What drives the distribution in nature of 3*T* *vs.* 2*M*₁ polytype in muscovites and phengites? A general assessment based on new data from metamorphic and igneous granitoid rocks. *American Mineralogist*, **95**, 1182–1191.

Schmidt M.W., Dugnani M. & Artioli G. (2001) Synthesis and characterization of white micas in the join muscovite-aluminoceladonite. *American Mineralogist*, **86**, 555–565.

Seifert F. (1968) X-ray powder data for Mg-A1-celadonite (leucophyllite) from Barcza, Poland. *Contributions to Mineralogy and Petrology*, **19**, 93–96.

Smoliar-Zviagina B.B. (1993) Relationships between structural parameters and chemical composition of micas. *Clay Minerals*, **25**, 603–624.

Smyth J.R., Jacobsen S.D., Swope R.J., Angel R.J., Arlt T., Domanik K. & Holloway J.R. (2000) Crystal structures and compressibilities of synthetic 2*M*₁ and 3*T* phengite micas. *European Journal of Mineralogy*, **12**, 955–963.

Sokolova T.N., Drits V.A., Sokolova A.L. & Stepanov S.S. (1976) Structural and mineralogical characteristics and conditions of formation of leucophyllite from salt-bearing deposits of Inder. *Litologia i Poleznye Iskopaemye*, **6**, 80–95 (in Russian).

Środoń J. & Eberl D.D. (1984) Illite. Pp. 495–544 in: *Micas* (S.W. Bailey, editor). Reviews in Mineralogy, **13**. Mineralogical Society of America, Washington, DC, USA.

Środoń J., Paszkowski M., Drygant D., Anczkiewicz A. & Banas M. (2013) Thermal history of Lower Paleozoic rocks on the Peri-Tornquist margin of the East European Craton (Podolia, Ukraine) inferred from combined XRD, K-Ar, and AFT data. *Clays and Clay Minerals*, **61**, 107–132.

Stöckert B. (1985) Compositional control on the polymorphism (2*M*₁–3*T*) of phengitic white mica from high pressure parageneses of the Sesia Zone (lower Aosta valley, Western Alps; Italy). *Contributions to Mineralogy and Petrology*, **89**, 52–58.

Tsipursky S.I. & Drits V.A. (1977) Effectivity of the electronic method of intensity measurement in structural investigation by electron diffraction. *Izvestija Akademii Nauk SSSR, Serija Fiziko-Matematicheskaja*, **41**, 2263–2271 (in Russian).

Velde B. (1965) Phengite micas: synthesis, stability, and natural occurrence. *American Journal of Science*, **263**, 886–913.

Vidal O. & Parra T. (2000) Exhumation paths of high-pressure metapelites obtained from local equilibria for chlorite–phengite assemblages. *Geological Journal*, **35**, 139–161.

Wilson M.D. (2013) *Rock-Forming Minerals, Volume 3C, Sheet Silicates: Clay Minerals*. The Geological Society, London, UK, 724 pp.

Zviagina B.B. & Drits V.A. (2012) Structural regularities in 2*M*₁ dioctahedral micas: the structure modeling approach. *American Mineralogist*, **97**, 1939–1954.

Zviagina B.B., Drits V.A., Środoń J., McCarty D.K. & Dorzhieva O.V. (2015) The illite–aluminoceladonite series: distinguishing features and identification criteria from X-ray diffraction and infrared spectroscopy data. *Clays and Clay Minerals*, **63**, 378–394.

Zviagina B.B., Drits V.A., Sakharov B.A., Ivanovskaya T.A. & Dorzhieva O.V. (2017) Crystal-chemical regularities and identification criteria in Fe-bearing, K-dioctahedral 1*M* micas from X-ray diffraction and infrared spectroscopy data. *Clays and Clay Minerals*, **65**, 234–251.